JOURNAL OF PROPULSION AND POWER
Vol. 15, No. 5, September–October 1999

Effect of Variable Axial Chord on a Low-Pressure Turbine Blade

C. G. Murawski*
U.S. Air Force Research Laboratory, Wright–Patterson Air Force Base, Ohio 45433-7251
and
K. Vafai†
Ohio State University, Columbus, Ohio 43210-1107

An experimental study was conducted in a two-dimensional linear cascade, with focus on the suction surface of a low-pressure turbine blade. Flow Reynolds numbers, based on exit velocity and suction surface length, were varied from 50,000 to 300,000. The axial chord of the blades was varied by tail extenders from 0 to 15% beyond design. The effects of Reynolds number on a low-pressure turbine cascade blade with tail extensions were investigated. Separation was observed at all Reynolds numbers and in all flow cases. This study has shown that for certain cases, changing the axial cord of a low-pressure turbine blade by use of tail extensions provided a clear improvement in boundary-layer behavior, which results in better overall blade performance. The most profound effect of the tail extensions was seen when the tail was short. There was no additional advantage when the tail extensions were longer than 6.1% of the axial chord. The shortest tail extension resulted in the greatest zone of performance enhancement. The longer tail extension resulted in a smaller region of performance enhancement.

Nomenclature

Cp	= local pressure coefficient $[(P_{T_{\text{in}}} - P_{\text{Si}})/\frac{1}{2}\rho U^2_{\text{OUT}}]$
P_{Si}	= static pressure along the blade surface
$P_{T_{\text{in}}}$	= total pressure at inlet of the blade set
$P_{T_{\text{out}}}$	= average total pressure behind the blade row
$P_{T_{\text{out},i}}$	= local total pressure behind the blade row
Re	= Reynolds number $[U_{\text{OUT}}\,(\text{SSL})/\nu]$
SSL	= suction surface length
Tu	= freestream turbulence intensity $(u'_{\text{rms}}/\bar{u}_{\text{local}})$
U_{OUT}	= average velocity out of the blade set
u'_{rms}	= root mean square of fluctuating component of streamwise velocity
$\bar{u}_{\text{local}}$	= local mean streamwise velocity
γ	= loss coefficient
ν	= kinematic viscosity
ρ	= density

Introduction

IN aircraft gas turbine engines, low-pressure turbine blade performance changes as the aircraft operates from takeoff to cruise. The low-pressure turbine experiences large changes in the chord Reynolds number because of reduced pressures while maintaining relatively high temperatures during high-altitude cruise conditions. A performance degradation is caused by the decrease in the flow Reynolds numbers as the aircraft operates at high-altitude cruise conditions. As the Reynolds number drops, flow separation zones expand and regions of transitional flow lengthen. The end result is a degradation in performance.[1] The changes in Reynolds number, strong acceleration of the flow on the blade, and large regions of uncovered diffusion can result in unsteady separation and transition zones on the surface of the blade.

Mayle,[2] in a review of the role of laminar to turbulent transitions in gas turbine engines, defined three modes of transition: natural transition, bypass transition, and separated-flow transition. Natural transition is defined by the classical development and breakup of Tollmien–Schlichting waves. Bypass transition skips over the formation of Tollmien–Schlichting linear instability waves, advancing directly to turbulent spots that eventually merge to yield a turbulent boundary-layer. Separated-flow transition occurs when a boundary layer separates, and transition proceeds in the free-shear-layer flow above the separation bubble. The transition region propagates toward the wall, giving a growing turbulent zone until the flow reattaches as a fully turbulent boundary layer. Because of the elevated levels of freestream turbulence, curvature, and the diffusion in the boundary layer, the transition processes most likely to occur on a turbine blade are bypass and separated-flow transition.

Halstead et al.[3] reported the results of an extensive experimental study of compressor and low-pressure turbine flows. Although their experiment concentrated on turbine flow that contained wake disturbances, they concluded that the performances of highly loaded, low-pressure turbine blades are dependent on flow transition and separation behavior. Murawski et al.[4] reported the results of an experimental study in which the two-dimensional cascade was used. Their low-pressure turbine blade was susceptible to large regions of separation as the Reynolds number was reduced. Decreases in the Reynolds number resulted in an earlier point of separation and larger separation zones. It was also shown that all the separation behavior occurs in the uncovered turning region of the suction side of the airfoil.

Rivir et al.[5] conducted a computational study of the Langston turbine cascade at Reynolds numbers relevant to low-pressure turbines. Their results show that the flow over the suction side of the Langston profile separates as the Reynolds number decreases below 100,000. They extended the tail of their computational blade, thus decreasing the region of uncovered turning. This change in blade shape resulted in a significant decrease in the size of the separation region. The reattachment point moved forward, resulting in a substantially smaller separation zone and wake width.

In the present work, the effects of changing the Reynolds number on a low-pressure turbine airfoil with a variable axial chord are investigated. The effects of varying the axial chord by use of tail extensions are documented by investigation of the suction-side pressure profile, boundary-layer surveys, and the loss coefficient variations at different Reynolds numbers.

Experimental Method

Experimental Apparatus

A linear, two-dimensional airfoil cascade was used to study a low-pressure turbine airfoil. A schematic of the test apparatus is

Received 4 May 1998; revision received 4 March 1999; accepted for publication 25 March 1999. Copyright © 1999 by C. G. Murawski and K. Vafai. Published by the American Institute of Aeronautics and Astronautics, Inc., with permission.

*Mechanical Engineer, Propulsion Directorate, Building 18, 1950 Fifth Street. Member AIAA.

†Professor, Department of Mechanical Engineering, 206 W. 18th Avenue. Associate Fellow AIAA.

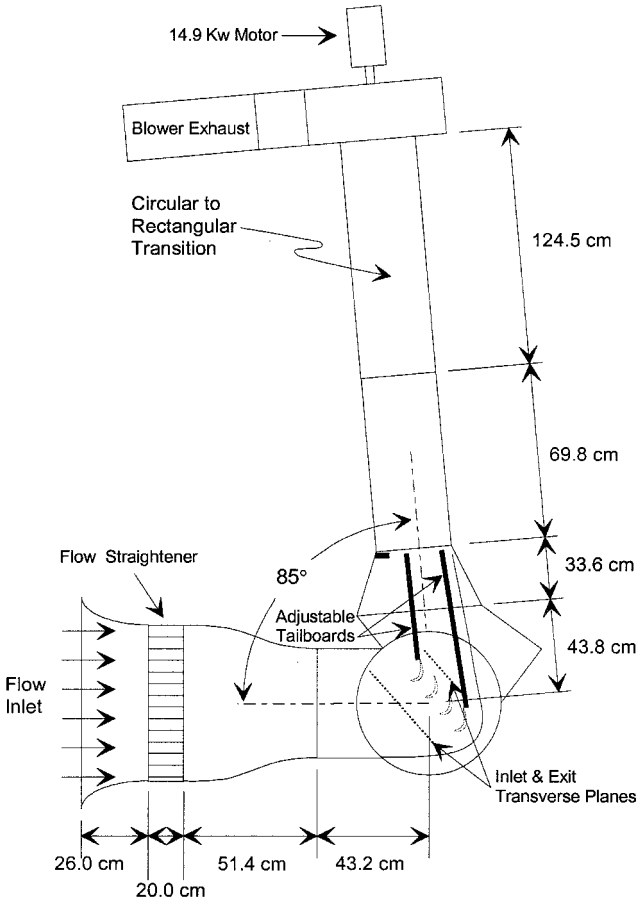

Fig. 1 Test apparatus.

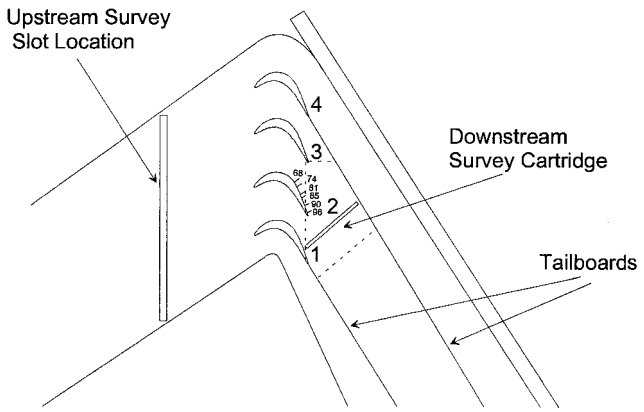

Fig. 2 Test section.

provided in Fig. 1. Air is pulled through the apparatus by a 20-hp motor operating a centrifugal blower in the suction mode. Air flow through the test rig is controlled by a variable-speed motor controller. The wind-tunnel-inlet bell mouth directs the flow through a 53 cm square × 20 cm deep honeycomb flow straightener. The flow continues through a 7:1 converging nozzle to the 11.4 cm × 40.6 cm flow channel.

The cascade used in this experiment is illustrated in Fig. 2. It contains four geometrically identical, low-pressure turbine blades with an axial chord length of 10.36 cm and a span-to-chord length aspect ratio of 1.1. The suction surface length is 15.24 cm. The pitch-to-chord ratio (solidity) is 0.88, and the flow is turned through 95 deg. The freestream turbulence in this experiment was not increased beyond normal tunnel turbulence. Inlet surveys are accomplished by insertion of instrumentation probes in a slot located 1.5 axial blade chords upstream of the leading edge of the test blades. Boundary-layer and downstream flow measurements were accomplished by insertion of a survey cartridge in the top wall. The survey cartridge contains a slot to enable the instrumentation probe to be traversed at the required location. Different survey cartridges may be utilized for each survey.

The cascade used in this experiment has an aspect ratio (blade height-to-blade pitch ratio) close to 1. Secondary flow is expected near the end walls. To establish that the secondary flow is not adversely influencing the two-dimensional flow region on the blade surfaces, the boundary layer and the static-pressure behavior of this cascade were compared with reported experimental results of Lake et al.[6] and Qiu and Simon.[7] Their turbine cascades contained the same blade geometry utilized in this paper, with aspect ratios greater than 5. The results of the present effort compared very favorably with the large aspect ratio cascades. The similar size and location of the separation bubble on the suction side of the turbine blade and its identical reaction to increasing Reynolds numbers clearly established that the cascade used in the present study contains a large enough two-dimensional region that is not significantly influenced by secondary flows.

The axial chord of the blades in the linear cascade was varied by the attachment of a length of 1.7-mm-thick Phenolic board to the tail at the design exit angle. The lengths of the tail attachments used in this experimental study are given in Table 1. These tail attachments were attached to blades 2 and 3. The axial chord was extended from 6.1 to 15.3% when these tail attachments were used. It should be noted that tailboards (not tail attachments) were added to blades 1 and 4 for directing the flow across the test section, as shown in Fig. 2.

Instrumentation

Instantaneous local velocities were measured with a single-element hot-wire probe. Boundary-layer profiles were recorded by traversing the single-element hot-wire probe at a 20-deg angle to the surface across the boundary layer. The wall is located by use of electrical continuity between the hot-wire probe tip and the wall. The distance from the hot wire to the wall was calculated and corrected by measurement of the tip diameter of the probe. Boundary-layer profiles were measured on a cascade blade at position 2, as illustrated in Fig. 2. The percentage of axial chord locations at which the traverses were recorded are annotated on blade 2.

Mean inlet velocity and total pressure measurements were made with a pitot-static probe. The airfoil surface–static pressures were measured with 22 static-pressure ports installed at midspan on the surface of one blade. The surface–static-pressure test blade was inserted in blade position 2 in the test section. The locations of the surface static pressure taps on the test blade are illustrated in Fig. 3. One pressure tap is located near the front stagnation point,

Table 1 Tail attachment data

Tail length, cm	0.0	1.27	1.90	2.54	3.17
Suction-side surface length, cm	15.24	16.51	17.14	17.78	18.41
Axial chord, cm	10.36	10.99	11.31	11.63	11.94
Change in axial chord	Base	+6.1%	+9.2%	+12.3%	+15.3%

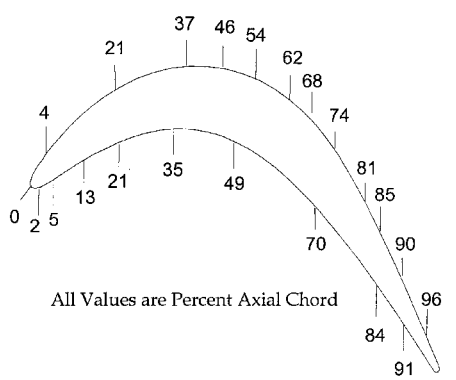

Fig. 3 Surface–static-pressure tap locations.

Table 2 Effect of variable axial chord: suction-side static-pressure and boundary-layer results[a]

Reynolds number	Tail length, cm	Maximum velocity	Terrace begins/ separation	Transition (terrace ends)	Terrace length	Reattachment
50,000	No tail	54	74/<74	85	11	96
	1.27	58	81/<81	90	9	96
	1.90	58	81/<81	90	9	>96
	2.54	62	81	90	9	——
	3.17	62	81	90	9	——
100,000	No tail	54	74/<74	85	11	96
	1.27	56	81/<81	85	4	96
	1.90	58	81/<81	85	4	96
	2.54	58	81	85	4	——
	3.17	60	81	85	4	——
200,000	No tail	54	68/>68	80	12	90
	1.27	54	74/>74	81	7	90
	1.90	58	74/>74	81	7	90
	2.54	58	74	81	7	——
	3.17	58	74	85	11	——
300,000	No tail	54	68	74	6	——
	1.27	56	74	81	7	——
	1.90	56	74	81	7	——
	2.54	58	74	81	7	——
	3.17	58	74	81	7	——

[a]Values for maximum velocity, terrace dimensions, and reattachment are given in terms of axial chord percentage.

nine surface-pressure taps are located on the pressure side of the test blade, and 12 static-pressure taps are located on the suction side of the test blade. It should be noted that the numbers cited on the blade in Fig. 3 refer to the percent axial chord. The ports are connected to stainless-steel tubing that manifolds to a Scanivalve selector. Three different Validyne pressure transducers were used to cover the range of cascade pressures. Voltages were acquired with a National Instruments Data Acquisition Board. National Instruments LabVIEW software was utilized for data acquisition.

The experimental uncertainties were determined based on the method of Kline and McClintock.[8] The uncertainty of the velocity measurements resulting from pressure transducers was calculated to be less than 2%. The maximum uncertainty in the pressure coefficient and loss coefficient were calculated to be less than 4%. The uncertainty of the velocity measurements from a single-wire, hot-wire anemometer was calculated to be less than 2%.

Results

Inlet Velocity Profile

To verify an acceptable inlet flow, a velocity survey was performed with a single-element hot-wire probe. The survey was taken with two blade chords upstream of the leading edges of the cascade blades at midtunnel height. The maximum variations from the mean inlet velocity for Reynolds number of 50,000, 100,000, and 200,000 were 3.57, 3.38, and 3.65%, respectively. The inlet freestream turbulence intensities for the Reynolds numbers listed above were 0.61, 0.54, and 1.08%, respectively.

Surface–Static-Pressure Surveys

Surface–static-pressure surveys were conducted on the two-dimensional cascade test blade for a wide range of Reynolds numbers. The results are presented in terms of a pressure coefficient defined by

$$Cp = \frac{\left(P_{T_{\text{in}}} - P_{\text{Si}}\right)}{\frac{1}{2}\rho U_{\text{OUT}}^2} \tag{1}$$

The method used to interpret the separation region on static-pressure coefficient plots over the pertinent portion of the suction side is illustrated in Fig. 4. This method is similar to that used by Gaster.[9] A region of the pressure plot that contains a flat zone or terrace is an indication of separated flow. The terrace is created by the initial portion of the separation bubble, which is composed of a laminar shear layer and a dead-air region. The magnitude of the velocity near the wall remains low as the shear layer interacts with the separation bubble. This mixing may result in boundary-layer reattachment. Toward the end of the separation bubble, the magnitude of the velocity will increase near the wall. Mayle[2] defined the end of transition as the knee on the static-pressure curve that begins to fall off quickly after the flat zone. Although the exact location of reattachment is not determined with these criteria, the boundary layers for each flow case can be compared by recording the beginning of the separation terrace and the beginning of the pressure recovery (the knee on the static-pressure curve) in the static-pressure plots. These observations are summarized in Table 2. It should be noted that Table 2 contains results from the surface–static-pressure surveys (location of maximum velocity, terrace beginning and end locations, and terrace length) and the boundary-layer hot-wire traverses (separation and reattachment).

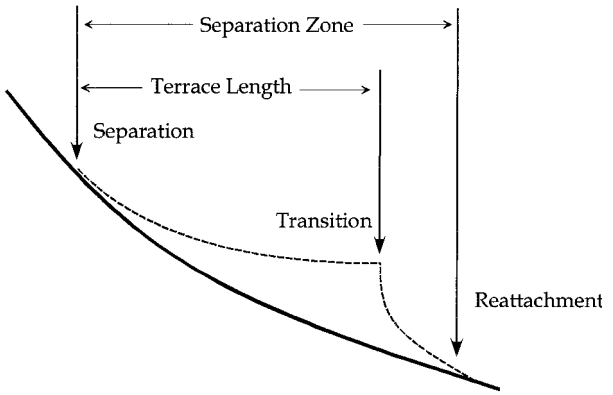

Fig. 4 Interpretation of the separation region on static-pressure plot over the pertinent portion of the suction side.

Figure 5 illustrates the surface–static-pressure survey for the cascade without tail extensions with varying Reynolds numbers. The pressure side is the lower portion of the plot. For all Reynolds numbers, the flow is attached for the whole length of the pressure side. The suction side is the top portion of the Fig. 5. The results show a separation occurring near 74% axial chord for Reynolds numbers less than 100,000. The point of separation moves forward as the Reynolds number is increased beyond 100,000. The location of the initiation of separation is affected for different values of Reynolds numbers. The location of the end of the static-pressure terrace, which is interpreted as the end of transition, also changes with Reynolds number. The terrace ends at ~85% axial chord for Reynolds number of 50,000. As the Reynolds number is increased, the end of the transition point moves forward. At a Reynolds number of 300,000, the flat terrace ends near 74% axial chord.

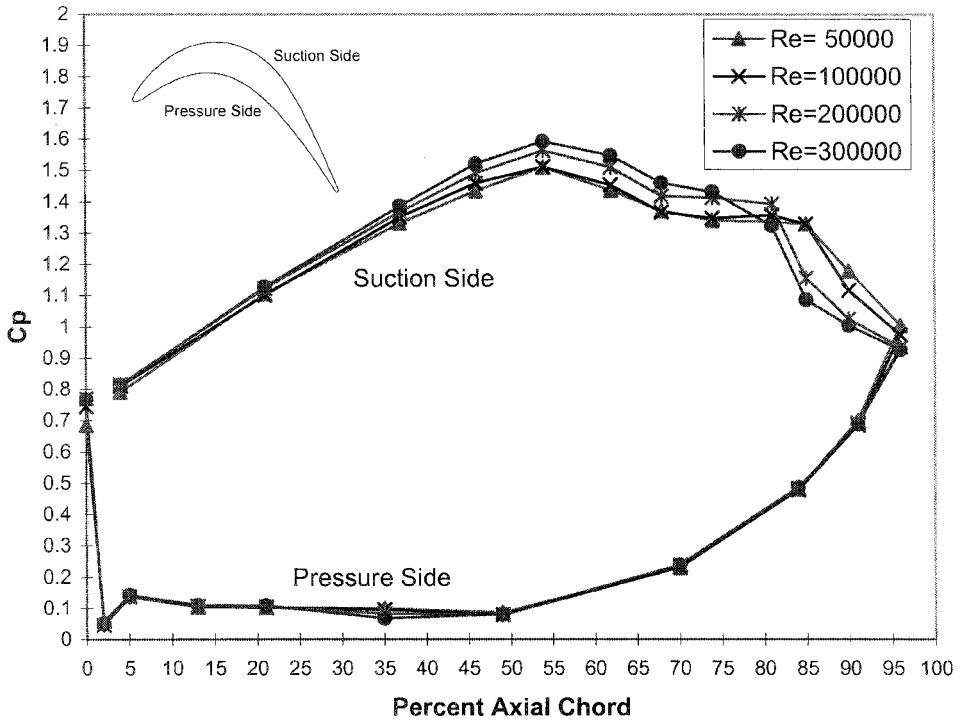

Fig. 5 Static-pressure survey, baseline.

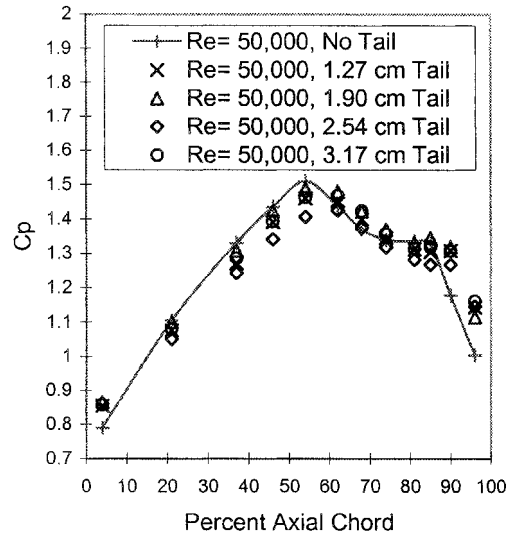

a) Re **= 50,000**

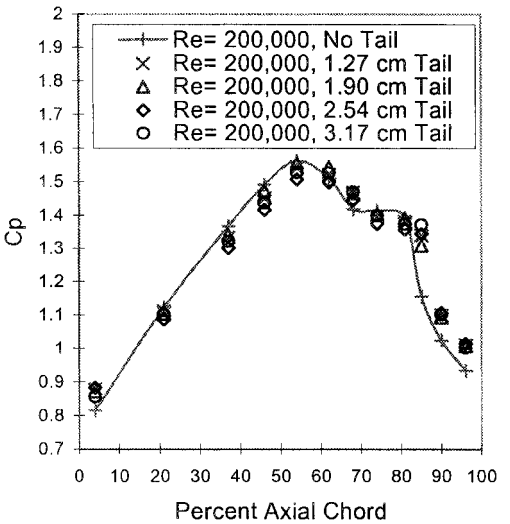

c) Re **= 200,000**

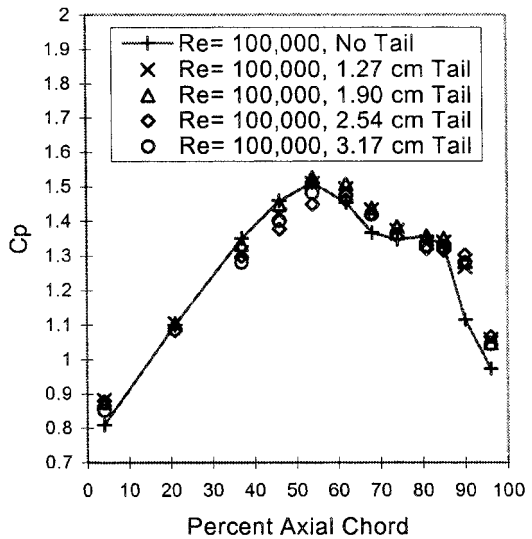

b) Re **= 100,000**

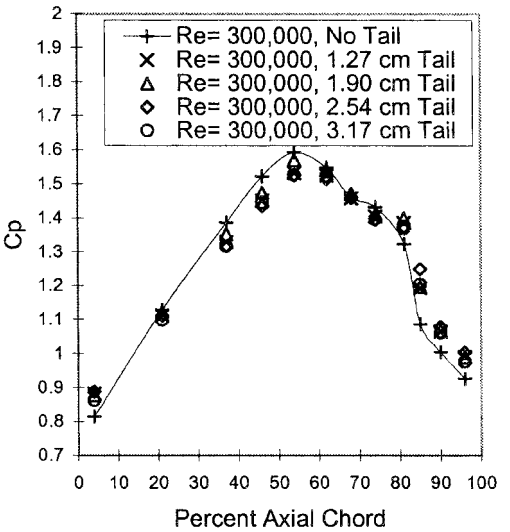

d) Re **= 300,000**

Fig. 6 Effect of variable axial chord on the static-pressure distribution on the suction side.

Figure 6 illustrates the results of the surface–static-pressure surveys for the suction side of the airfoil. Each plot contains the results of one Reynolds number and the effect of varying the axial chord. Figure 6a illustrates the results of the suction-side surface–static-pressure survey for a Reynolds number of 50,000. The solid curve represents the baseline blade with no tail extension. Adding a relatively short tail extension to the baseline blade delays the location of maximum velocity on the suction surface, delays the onset of separation, and decreases the separation zone size. The terrace length is decreased by 18%. Increasing the tail length for the case of Reynolds number of 50,000 does not change the terrace length any further. For this case, a short tail extension of ~6% will be adequate to provide the largest impact on the boundary layer.

Figures 6b and 6c illustrates the results of the suction-side surface–static-pressure surveys for Reynolds number of 100,000 and 200,000, respectively. The summary of results in Table 2 shows that the suction-side surface behaves similarly for this range of Reynolds number. The terrace length shrinks substantially compared with the case when no tail is attached. Separation moves rearward when a tail extension is attached to the baseline blade. Increasing the tail length does not have much of an impact on the point of separation. The terrace lengths on the static-pressure survey plots remain constant for tail lengths of 1.27, 1.90, and 2.54 cm.

The largest impact of the tail extensions was recorded for a Reynolds number of 100,000. Table 2 shows that for Reynolds number of 100,000, the short tail extension of 1.27 delays boundary-layer separation and decreases the terrace length by more than 75%. As the tail extension is increased beyond 2.54 cm, the terrace length, which corresponds to separation zone size, remains constant at less than half the length of the no-tail-extension case.

The results in Table 2 show that as the Reynolds number increases from 100,000 to 200,000 for the baseline case, without tail extension, the separation zone is similar in size as the whole separation bubble moves forward on the suction-side blade surface. When the shorter tail extensions are added to the blade at a Reynolds number of 200,000, the terrace length on the static-pressure survey shrinks by about half. However, when the tail extension is increased to 3.17 cm, the size of the terrace increases almost back to the baseline length. This occurs even though the location of separation, the point at which the terrace begins, is moved downstream from 68% axial chord to 74% axial chord. The advantage gained by tail attachments is constant after exceeding a certain attachment length, as seen in Fig. 6c and Table 2. This gives an indication for the existence of an optimized tail length for a given range of Reynolds numbers. For the low-pressure turbine blade utilized in the present investigation the greatest impact on the suction-side boundary layer was seen when the tail extension lengths were ~6% of axial chord.

Figure 6d illustrates the results of the suction-side surface–static-pressure survey for Reynolds number of 300,000. In this case the tail attachments have the effect of delaying the point of maximum velocity and the onset of separation. The length of the terrace, which is an indication of the length of separation, is hardly influenced by the tail attachments. Table 2 shows the terrace length as growing by 1% axial chord when tails are attached. This change in terrace length is not significant. This indicates that the impact of the tail attachments is diminished for larger Reynolds numbers.

Boundary-Layer Survey

Boundary-layer profiles were obtained for the baseline (no tail extension), 1.27-, and 1.90-cm tail attachment cases for Reynolds numbers of 50,000, 100,000, and 200,000. The static-pressure surveys established that the greatest performance enhancement was when tail attachments of 9.2% of the axial chord or less were utilized. The static-pressure surveys were able to show the point of separation and the end of the transition on the suction-side boundary layer. The suction-side boundary-layer reattachment point could not be determined accurately from the surface–static-pressure surveys. To determine the reattachment point, a boundary-layer survey was conducted. The results of the boundary-layer survey are summarized in Table 2. Detailed velocity profiles and local turbulence intensities were recorded within the boundary layer. Interpretation of the boundary layer surveys was similar to that used by Murawski et al.[4] and Qiu and Simon.[7]

Figure 7 shows the results of the boundary-layer velocity survey for the three tail configurations with a Reynolds number of 50,000. Separation occurs for the baseline, no-tail case at ~74% axial chord. Separation of the boundary layer is delayed when tail extensions are added. Figure 8 shows the local turbulence-intensity distribution within the boundary layer for different tail extensions. Laminar-attached flow is a region in which the local turbulence intensity remains below 10%. Separated flow appears as a turbulence-intensity curve in which the peak turbulence intensity is not at the wall, but occurs in the shear layer on top of the separation bubble. The attached turbulent boundary layer appears as a curve where the maximum turbulence intensity occurs near the wall and values of turbulence intensity decrease away from the wall. For all cases, the boundary layer is attached at 68% axial chord. At 74% axial chord, the boundary has separated for the no-tail case, whereas the boundary layer remained attached for the 1.27- and 1.90-cm tail extension cases. At 81% axial chord all the boundary layers in Figs. 7 and 8 are separated, whereas the baseline case has been separated before the 74% axial chord. The separation region can be seen as the chord section over which zero velocity gradient at the wall exists and appears as a large low-velocity region on the velocity profiles.

It appears at first that the 1.90-cm tail results in a better-behaved boundary layer by delaying the separation point. However, at 96% axial chord, although the velocity profiles (Fig. 7) appear very similar, the boundary-layer turbulence intensity (Fig. 8) reveals the actual state of the boundary layer. For the baseline case, at 96% axial chord, the flow has either just attached or is about to attach as a turbulent boundary layer. For the 1.27-cm tail case, the flow is clearly attached because the local turbulence intensity is highest at the wall and falls away quickly as distance from the wall is increased. For the 1.90-cm case, at the 96% axial chord, the boundary layer is not yet attached, but attachment will occur soon because the high turbulence intensity has diffused toward the wall. For a Reynolds number of 50,000, it

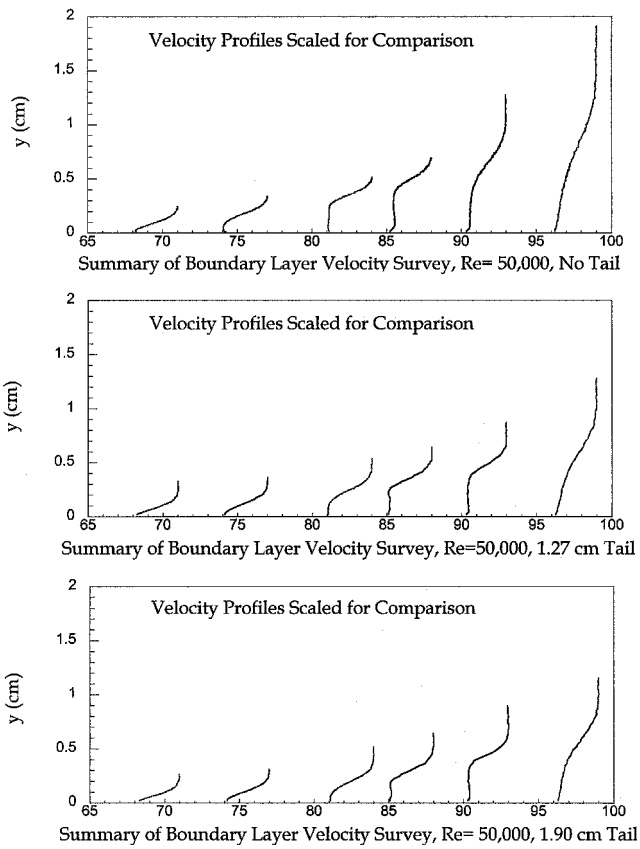

Fig. 7 Velocity distribution at different axial chord locations along the blade suction side for *Re* = 50,000.

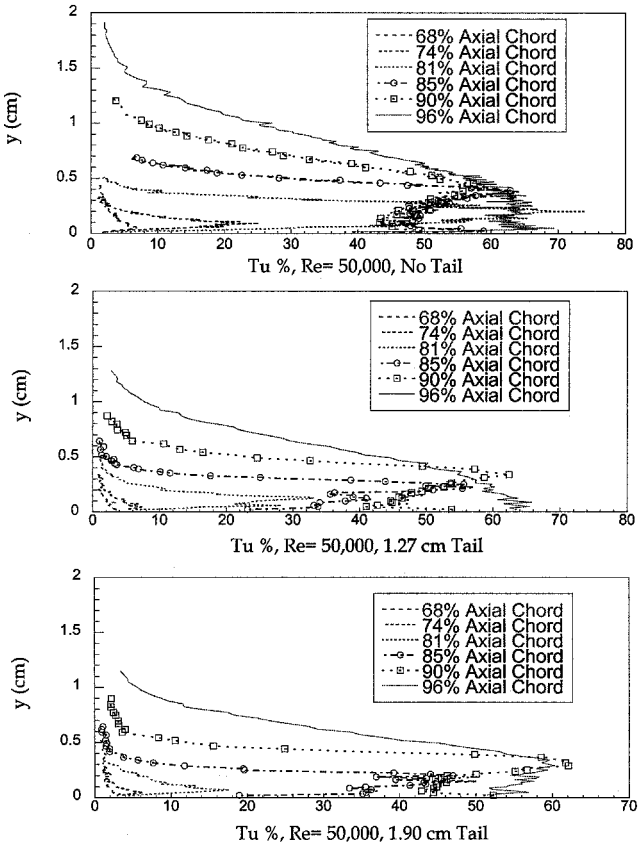

Fig. 8 Turbulence level distribution at different axial chord locations along the blade suction side for *Re* = 50,000.

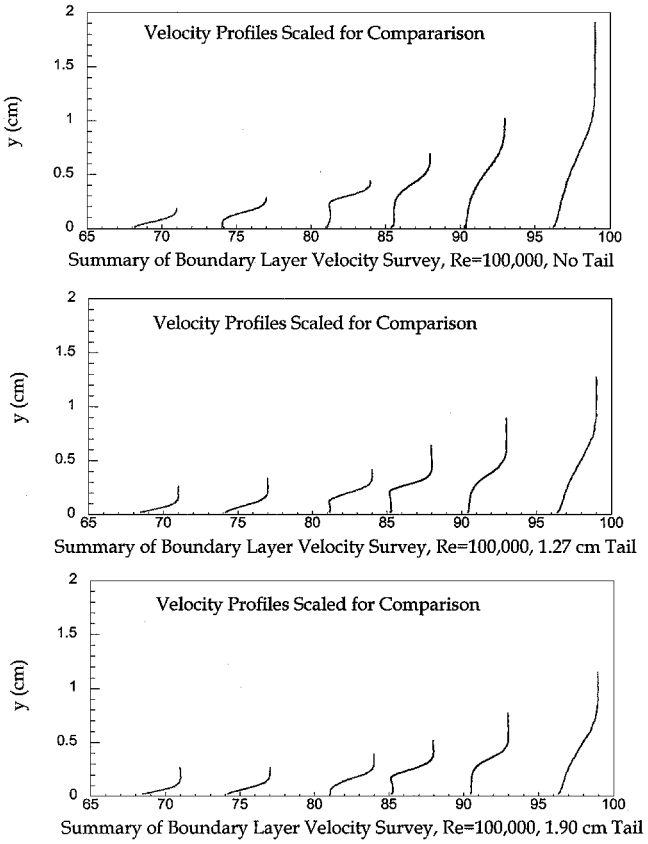

Fig. 9 Velocity distribution at different axial chord locations along the blade suction side for *Re* = 100,000.

can be concluded that increasing the axial chord by 6.1%, by use of a tail attachment, results in a delayed and smaller separation region. The 1.90-cm tail delays the separation further downstream compared with the 1.27-cm tail case; however, the shorter tail results in a shorter separation zone.

Figures 9 and 10 illustrate the velocity and the freestream turbulence distributions, respectively, for a Reynolds number of 100,000. For the baseline case, i.e., no tail extension, the flow has separated at 74% axial chord and has reattached at 96% axial chord. For the 1.27- and the 1.90-cm tail extensions, the boundary-layer separation is delayed until before 81% axial chord, and the reattachment occurs before the 96% axial chord marker. For a Reynolds number of 100,000, it can be seen that using the shorter 1.27-cm tail is adequate (Table 2) in providing a meaningful performance enhancement on the low-pressure turbine airfoil. Using a longer tail extension will not provide a greater performance enhancement.

The boundary-layer surveys for a Reynolds number of 200,000 are illustrated in Figs. 11 and 12. As can be seen in Fig. 11, the boundary layer for the baseline case (no tail extension) separates after the 68% axial chord marker. Once again, the tail extension cases delay the separation point. In this case the separation point is delayed until after the 74% axial chord location. The similarity between the boundary-layer freestream turbulence levels (Fig. 12) for the baseline and the tail extension cases indicates that the reattachment point is not affected by the addition of the tail extensions. For the baseline case as well as the tail extension attachment cases the boundary layers are attached around the 90% axial chord marker. Therefore the use of a variable axial chord turbine blade provides only a minimal performance enhancement for a Reynolds number of 200,000.

For all Reynolds numbers, it can be seen from Figs. 7, 9, and 11 that, based on observation of the length of the flat portion of the velocity profile, the height of the separation bubble decreases when tail extensions are attached to the test blade. The height of the separation bubble decreases slightly as the tail extension increases from 6.1 to 9.2%.

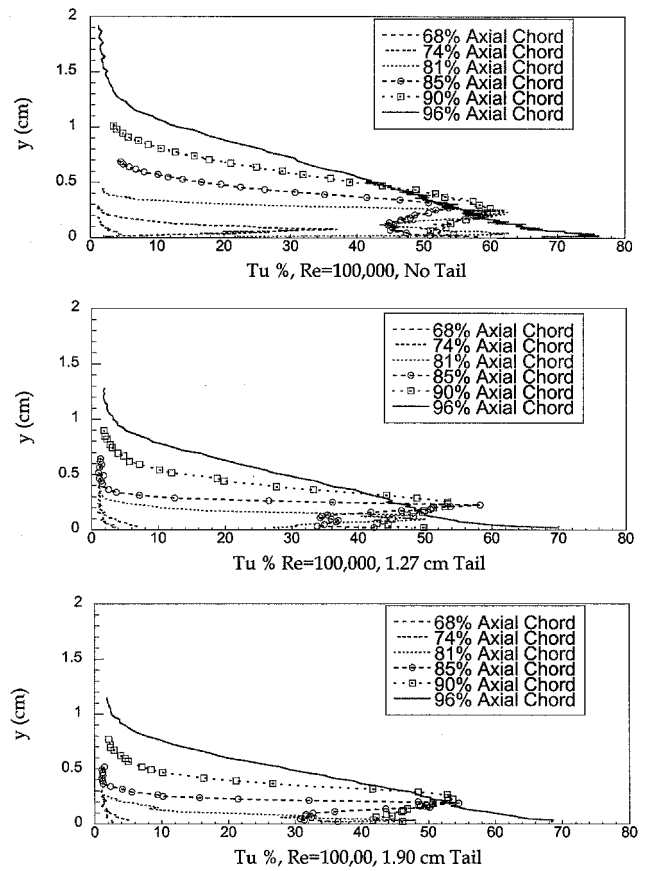

Fig. 10 Turbulence level distribution at different axial chord locations along the blade suction side for *Re* = 100,000.

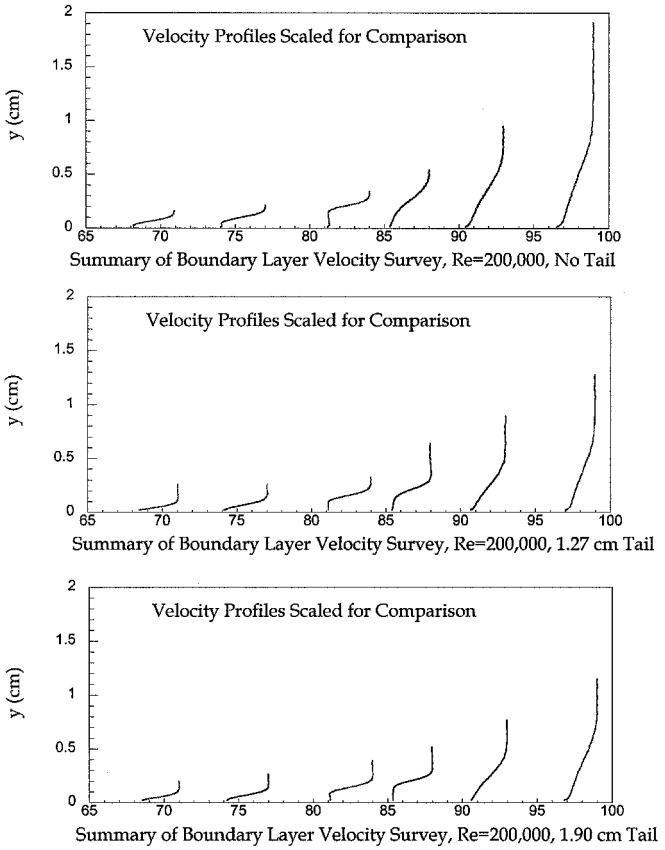

Fig. 11 Velocity distribution at different axial chord locations along the blade suction side for *Re* = 200,000.

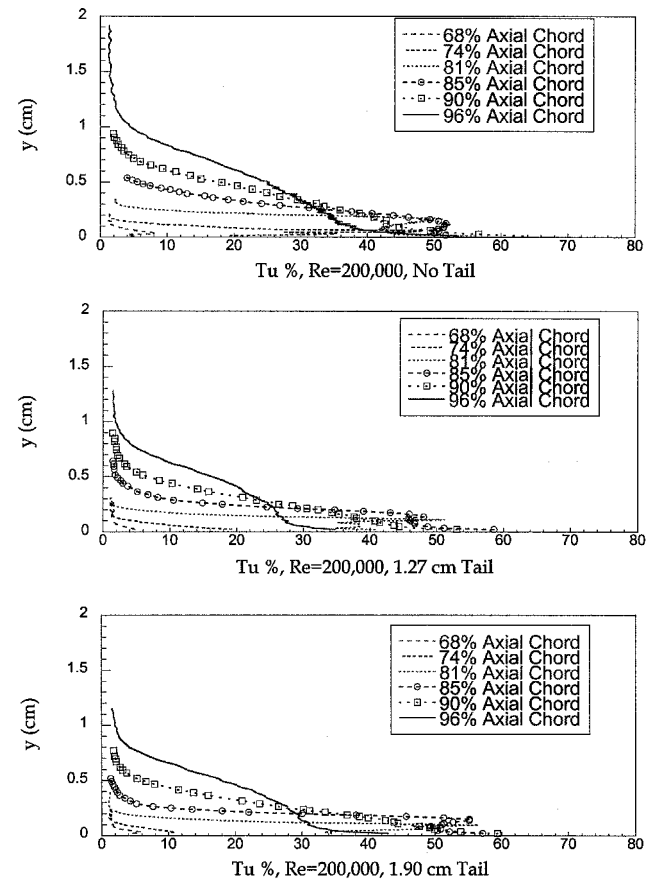

Fig. 12 Turbulence level distribution at different axial chord locations along the blade suction side for *Re* = 200,000.

The flow separation on the suction-side boundary layer occurs in the area of uncovered turning or uncovered diffusion. The aft portion of the turbine blade is where the majority of flow diffusion occurs without the direct control of the pressure sidewall of the opposing blade. The static-pressure plots and the boundary-layer results without any tail extensions show that this is the region where the boundary-layer separation behavior takes place. The addition of the tail extensions decreases the region of uncovered diffusion, which delays the onset of boundary-layer separation on the suction side. Also the tail extensions decrease the height of the separation bubble. This smaller separation zone results in less blade profile drag and a decrease in the extent of shear layer mixing over the separation bubble. These factors contribute to better overall blade performance at lower Reynolds numbers. The boundary-layer reattachment point, which remains in the uncovered turning region, is not affected by the presence of the tail extensions.

Loss Coefficient

Overall performance is documented with the loss coefficient:

$$\gamma = \frac{\left(P_{T_{\text{in}}} - \overline{P_{T_{\text{out}}}}\right)}{\frac{1}{2}\rho U_{\text{OUT}}^2} \tag{2}$$

In this work, the inlet total pressure is measured two axial blade chords upstream, whereas the outlet total pressure, which is the average of a traverse perpendicular to the exit flow, is measured at 25% of axial chord downstream of the test blade. Figure 13 shows the loss coefficients for the blade set without tail attachments as well as the blade set with 1.27- and 1.90-cm tail attachments. Figure 13 shows that for all cases the overall blade losses decrease as Reynolds numbers increase. The 1.27-cm tail attachment resulted in higher loss coefficients when the Reynolds number was 300,000. The 1.27-cm tail attachment results in a better performance for Reynolds numbers less than 200,000. This is the range usually specified as the cruise condition for a low-pressure turbine. Above a Reynolds number of 200,000, both the 1.27- and 1.90-cm tail extensions resulted in a larger loss coefficient than that of the base case. The 1.90-cm tail extension shows a performance improvement within a smaller range confined to a Reynolds number of ~100,000. The shorter 1.27-cm tail returns lower loss coefficients for a Reynolds number range from 50,000 to ~200,000. This is a much greater range compared with that of the longer tail extension case. Loss coefficients were not recorded for tails longer than 1.90 cm because Table 2 showed that longer tail attachments resulted in no improvement in reducing the extent of the separation zone for the majority of cases.

Figure 13 shows that this low-pressure turbine was designed to have optimal performance at Reynolds numbers of 300,000 or greater. The addition of tail extensions changes the blade solidity (axial chord-to-blade pitch ratio) and changes the region of uncovered turning. At the higher Reynolds numbers this results in higher overall losses. A large boundary-layer separation is observed on the

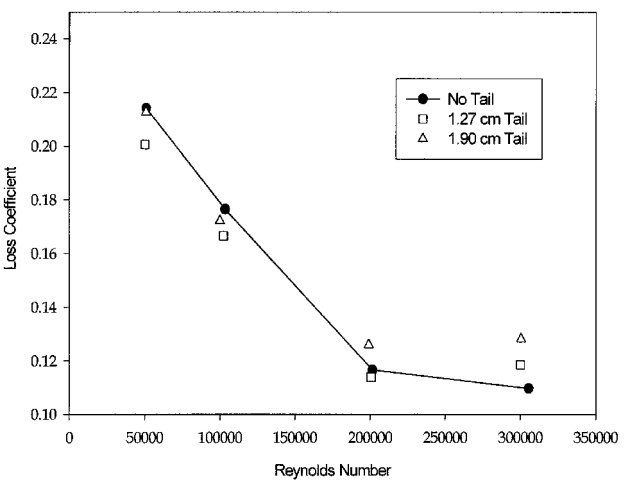

Fig. 13 Loss coefficient variations at different Reynolds numbers.

suction side of the blade, in the region of uncovered diffusion at lower Reynolds numbers. The change in blade geometry from the addition of tail extensions leads to lower overall losses at the lower Reynolds numbers.

Conclusions

In the present study, the effects of Reynolds number on a low-pressure turbine cascade blade with variable axial chord was investigated. Separation was observed at all Reynolds numbers and in all flow cases in this experimental study. It has been established that tail extensions provide a clear improvement in suction-side boundary-layer behavior, which can result in a better blade performance. The most profound effect of the tail extensions was seen when the tail extension was relatively short. There was no additional advantage when the tail extension was longer than ~6.1% of axial chord, and in fact, in some cases, the performance was downgraded for a longer tail extension.

It was found that the tail extensions tend to delay the separation point on the suction side of the low-pressure turbine blade. For a Reynolds number of less than 300,000, the size of the separation zone is substantially affected by the presence of the tail extensions. The shortest tail extension resulted in the greatest zone of performance enhancement on the loss coefficient in the range of Reynolds numbers from 50,000 to 200,000. The longer tail extensions resulted in a smaller region of performance enhancement. The tail extensions resulted in larger losses at Reynolds numbers beyond 200,000.

The addition of tail extensions changes the blade solidity (axial chord-to-blade pitch ratio) and changes the region of uncovered turning. At higher Reynolds numbers, this resulted in higher overall losses. However, at lower Reynolds numbers, the addition of the tail extensions, which decreased the region of uncovered diffusion, delayed the onset of boundary-layer separation on the suction side and decreased the height of the separation bubble. This smaller separation zone resulted in less blade profile drag and a decrease in the extent of shear layer mixing over the separation bubble. These factors contributed to lower losses and better overall blade performance at lower Reynolds numbers.

Acknowledgments

The authors are grateful for the professional assistance and advice from members of the U.S. Air Force Research Laboratory Basic Aerothermal Research Program. The authors are grateful for the support of Paul King of the U.S. Air Force Institute of Technology Aeronautical Engineering Department for use of the linear cascade. The authors also acknowledge the help of the U.S. Air Force Institute of Technology model shop and the University of Dayton, Dayton, Ohio, Department of Mechanical Engineering machine shop.

References

[1]Sharma, O. P., Ni, R. H., and Tanrikut, S., "Unsteady Flows in Turbines—Impact on Design Procedure," AGARD-LS-195, Paper 5, 1994.

[2]Mayle, R. E., "The Role of Laminar–Turbulent Transition in Gas Turbine Engines," ASME Paper 91-GT-282, American Society of Mechanical Engineers, New York, 1991.

[3]Halstead, D. E., Wisler, D. C., Okiishi, T. H., Walker, G. J., Hodson, H.P., and Shin, H.-W., "Boundary Layer Development in Axial Compressors and Turbines, Part 4 of 4: Computations and Analysis," ASME Paper 95-GT-464, American Society of Mechanical Engineers, New York, 1995.

[4]Murawski, C. G., Sondergaard, R., Rivir, R. B., Vafai, K., Simon, T. W., and Volino, R. J., "Experimental Study of the Unsteady Aerodynamics in a Linear Cascade with Low Reynolds Number Low Pressure Turbine Blades," ASME Paper 97-GT-95, American Society of Mechanical Engineers, New York, 1997.

[5]Rivir, R., Sondergaard, R., Dahlstrom, M., and Ervin, E., "Low Reynolds Number Turbine Blade Cascade Calculations," *ISROMAC-6, Proceedings of the Sixth International Symposium on Transport Phenomena and Dynamics of Rotating Machinery*, Vol. 2, Turbo and Power Machinery Research Center, Seoul, Korea, 1996, pp. 132–141.

[6]Lake, J. P., King, P. I., and Rivir, R. B., "Reduction of Separation Losses on a Turbine Blade with Low Reynolds Numbers," AIAA Paper 99-0242, Jan. 1999.

[7]Qiu, S., and Simon, T.W., "An Experimental Investigation of Transition as Applied to Low Pressure Turbine Suction Surface Flows," ASME Paper 97- GT-455, American Society of Mechanical Engineers, New York, 1977.

[8]Kline, S. J., and McClintock, F. A., "Describing Uncertainties in Single-Sample Experiments," *Mechanical Engineering*, Vol. 75, 1953, pp. 3–8.

[9]Gaster, M., "The Structure and Behavior of Laminar Separation Bubbles," (Separated Flows), CP-4, AGARD, 1966, pp. 819–854.